ASTRONOMY & ASTROPHYSICS
SUPPLEMENT SERIES

Astron. Astrophys. Suppl. Ser. **132**, 107–119 (1998)

The art of fitting p-mode spectra

I. Maximum likelihood estimation

T. Appourchaux[1], L. Gizon[1,2], and M.-C. Rabello-Soares[1,3]

[1] Space Science Department of ESA, ESTEC, NL-2200 AG Noordwijk, The Netherlands
[2] W.W. Hansen Experimental Physics Laboratory, Center for Space Science and Astrophysics, Stanford University, Stanford, CA 94305-4085, U.S.A.
[3] Teoretisk Astrofysik Center, Århus Universitet, DK-8000 Århus C, Denmark

Received October 17, 1997; accepted March 24, 1998

Abstract. In this article we present our state of the art of fitting helioseismic p-mode spectra. We give a step by step recipe for fitting the spectra: statistics of the spectra both for spatially unresolved and resolved data, the use of Maximum Likelihood estimates, the statistics of the p-mode parameters, the use of Monte-Carlo simulation and the significance of fitted parameters. The recipe is applied to synthetic low-resolution data, similar to those of the LOI, using Monte-Carlo simulations. For such spatially resolved data, the statistics of the Fourier spectrum is assumed to be a multi-normal distribution; the statistics of the power spectrum is *not* a χ^2 with 2 degrees of freedom. Results for $l = 1$ shows that all parameters describing the p modes can be obtained with negligible bias and with minimum variance provided that the leakage matrix is known. Systematic errors due to an imperfect knowledge of the leakage matrix are derived for all the p-mode parameters.

Key words: methods: analytical; data analysis; statistical — Sun: oscillations

1. Introduction

In the past decade, helioseismology has been able to provide the internal structure of the Sun and its dynamics. These inferences have been made possible by inverting the frequencies and rotational splitting of the pressure modes. The most commonly used technique for obtaining the p-mode parameters is to fit the p-mode spectra using Maximum Likelihood Estimators (MLE) assuming that the statistical distribution of the p modes in the power spectra is a χ^2 with 2 degrees of freedom (Woodard 1984). The MLE with this statistics were first applied on helioseismology data by Duvall & Harvey (1986) and Anderson et al. (1990). This technique is used for fitting spectra obtained with integrated sunlight instruments. For low- or high-resolution instruments, the (m, ν) power spectra are commonly fitted assuming that each m spectrum has the same statistics as the for the integrated sunlight instruments (LOI instrument: Appourchaux et al. 1995; Rabello-Soares et al. 1997; GONG instrument: Hill et al. 1996). Unfortunately, none of these implementations are correct since the assumed statistics is wrong. Only Schou (1992) described a more correct way of fitting (m, ν) diagrammes using *not* the power spectra but the complex Fourier spectra.

The pioneering work of Schou (1992) has inspired this series of 3 articles for addressing our state of the art of fitting (m, ν) diagrams. In this paper (Part I), we describe the statistics of the p modes, and how the MLE can be used in helioseismology. In Appourchaux et al. (1997) (hereafter Part II), we show how one can measure the mode leakage matrix and the noise correlation from the data which knowledge is required for using the Part I. In Appourchaux & Gizon (1998) (hereafter Part III), we will apply these techniques to the LOI instrument of VIRGO on board SOHO (For a description of the performance of the instrument see Appourchaux et al. 1997).

In this paper, we explain how the MLE can be used in helioseismology. In the first section, we recall the properties of MLE. In the second section, we describe the statistics of the p-mode Fourier spectra. In this section, we have generalized the approach of Schou (1992), to any complex leakage matrices. We have also used complex matrices to generate the covariance matrices of the p modes and of the noise. In the third section we show how to use Monte-Carlo simulations for testing both the use of MLE and the model of the p-mode spectra, and then conclude.

Send offprint requests to: thierrya@so.estec.esa.nl

2. Maximum likelihood estimators

Some of the properties of MLE were given by Toutain & Appourchaux (1994). We repeat them here for completeness. We also address 2 issues that were not covered in their paper: are MLE biased?, and how significant are the estimated parameters.

2.1. Fundamental properties

The aim of this section is to introduce some definitions and properties of MLE. A comprehensive study of this area of statistics can be found, e.g. in Kendall & Stuart (1967). Given a random variable x with a probability distribution $f(x, \boldsymbol{\lambda})$, where $\boldsymbol{\lambda}$ is a vector of p parameters. We define the logarithmic likelihood function ℓ of N independent measurements x_k of x as

$$\ln L = \ell = -\sum_{k=1}^{N} \ln f(x_k, \boldsymbol{\lambda}). \tag{1}$$

where L is the likelihood. The main property of ℓ is that the position of its minimum in the $\boldsymbol{\lambda}$-space gives an estimate of the most likely value of $\boldsymbol{\lambda}$, denoted hereafter as $\tilde{\boldsymbol{\lambda}}$. Hence $\tilde{\boldsymbol{\lambda}}$ is the solution of the set of p simultaneous equations:

$$\frac{\partial \ell}{\partial \lambda_i} = 0 \text{ with } i = 1, 2, ..., p. \tag{2}$$

Moreover, in the limit of very large sample ($N \to \infty$) this estimator $\tilde{\boldsymbol{\lambda}}$ tends to have a multi-normal probability distribution. In this case, this estimator is asymptotically unbiased with minimum variance; which implies its expectation and variance are respectively:

$$\lim_{N\to\infty} E(\tilde{\boldsymbol{\lambda}}) = \boldsymbol{\lambda}. \tag{3}$$

$$\lim_{N\to\infty} \sigma^2(\tilde{\boldsymbol{\lambda}}) = c_{ii} \tag{4}$$

where c_{ii} are the diagonal elements of the inverse of the Hessian matrix h, with elements:

$$h_{ij} = E(\frac{\partial^2 \ell}{\partial \lambda_i \partial \lambda_j}). \tag{5}$$

The covariances between any 2 components of $\tilde{\boldsymbol{\lambda}}$ are given by the corresponding off-diagonal elements of the inverse matrix. Equation (5) is used when computing the so-called formal error bars on $\tilde{\boldsymbol{\lambda}}$; as a matter of fact according to the Cramer-Rao theorem, Eq. (5) gives only a lower bound to the error bars (Kendall & Stuart 1967, reference therein). Toutain & Appourchaux (1994) showed that Eq. (5) is valid for most purpose in helioseismology.

2.2. Biased or unbiased?

The fact that MLE are asymptotically unbiased does not necessarily mean that this property is kept for a finite amount of data. As an example, it is well known that an estimator of the standard deviation (σ) of N measurement of a normally distributed random variable x is given by:

$$\sigma^2 = \frac{1}{N-1} \sum_{i=1}^{N} (x_i - \tilde{m})^2 \tag{6}$$

where x_i is the i-th measurement of the random variable x and $\tilde{m}$ is an estimate of the mean. It is well known that the σ of Eq. (6) is unbiased. In this case, MLE would give the following estimator:

$$\sigma^2_{\mathrm{MLE}} = \frac{N-1}{N} \sigma^2 \tag{7}$$

Clearly the MLE expression give a bias that vanish asymptotically for an infinite number of points. It is often difficult to derive explicit relation, similar to Eq. (7) between the estimator and the finite number of data points. When analytical expression can not be found, we advice to use Monte-Carlo simulations to verify the unbiasness; an example for $l = 1$ splittings is given in Chang (1996) and Appourchaux et al. (1997).

In any case MLE are intrinsically biased estimators because they are also minimum variance estimators (Kendall & Stuart 1967). It may be useful to find other estimators that do not bias the estimates (Quenouille 1956); they might not necessarily have minimum variance. These estimators are yet to be found.

2.3. Significance of fitted parameters

When one uses Least Square for fitting data, one can test the significance of its fitted parameters using the so-called R test (Frieden 1983). For MLE, a useful test can be used: the likelihood ratio test. It was first used by Appourchaux et al. (1994). This method requires to maximize the likelihood $\mathrm{e}^{-\ell(\omega_p)}$ of a given event where p parameters are used to described the line profile. If one wants to describe the same event with n additional parameters, the likelihood $\mathrm{e}^{-\ell(\Omega_{p+n})}$ will have to be maximized. The likelihood ratio test consists in making the ratio of the two likelihood (Brownlee 1965). Using the logarithmic likelihood, we can define the ratio Λ as:

$$\ln(\Lambda) = \ell(\Omega_{p+n}) - \ell(\omega_p). \tag{8}$$

If Λ is close to 1, it means that there is no improvement in the maximized likelihood and that the additional parameters are not significant. On the other hand, if $\Lambda \ll 1$, it means that $\ell(\Omega_{p+n}) \ll \ell(\omega_p)$ and that the additional parameters are very significant. In order to define a significance for the n additional parameters, we need to know the statistics of $\ln(\Lambda)$ under the null hypothesis, i.e. when the n additional parameters are not significant. For this null hypothesis, Wilks (1938) showed that for large sample size the distribution of $-2\ln\Lambda$ tends to the $\chi^2(n)$ distribution.

3. The statistics of p-mode spectra

3.1. Single mode

It is well known that p modes are stochastically excited oscillators (Kumar et al. 1988). The source of excitation lies in the many granules covering the Sun. The modes are assumed to be independently excited provided that their spatial scale is larger than the granule size (Chang 1996). From the equation of an oscillator, the statistics of the p-mode profile can be derived as:

$$\frac{\mathrm{d}^2x}{\mathrm{d}t^2} + 2\pi\gamma\frac{\mathrm{d}x}{\mathrm{d}t} + (2\pi)^2\nu_0^2 x = F(t) \tag{9}$$

where t is the time, x is the displacement, γ is the damping term or the linewidth, ν_0 is the frequency of the mode and $F(t)$ is the forcing function. From this equation the Fourier transform of x can be written as:

$$\tilde{x}(\nu) = \frac{\tilde{F}(\nu)}{(2\pi)^2(\nu_0^2 - \nu^2 + i\gamma\nu)} \tag{10}$$

where $\tilde{x}(\nu)$ and $\tilde{F}(\nu)$ are the Fourier transform of $x(t)$ and $F(t)$. From the large number of granules, it can be derived that the forcing function is normally distributed. Therefore the 2 components (the real and imaginary parts) of the Fourier transform of the forcing function are also normally distributed. For the p modes, each component of the Fourier transform is normally distributed with a mean of zero, and a variance given by:

$$\sigma^2(\nu) = \frac{1}{2}\frac{\sigma_{\tilde{F}}^2(\nu)}{(2\pi)^4[(\nu_0^2 - \nu^2)^2 + \nu^2\gamma^2]}. \tag{11}$$

The square of the modulus of $\tilde{x}(\nu)$, or power spectrum, has a χ^2 with 2 degree of freedom statistics and its mean is twice that of Eq. (11). This is the p-mode profile that is usually approximated by a Lorentzian profile. Similarly other effects such as asymmetry can be introduced in the profile of Eq. (11).

3.2. Unresolved observations

Instruments integrating over the solar surface the velocity or the intensity signal observe a superposition of various modes of different degrees. They are mainly sensitive to the low-degree modes ($l \leq 4$). For a given l, they detect a mixing of azimuthal order m for which a visibility is prescribed (Toutain & Gouttebroze 1994; Christensen-Dalsgaard & Gough 1982). Most often they can only detect modes for which $l+m$ is even. Since the Fourier components of the observed time series have a normal distribution, and since the different m are uncorrelated, the statistics of the power spectra of unresolved observation is a χ^2 with 2 degrees of freedom. Toutain & Appourchaux (1994) gave an analysis of the problem associated with these observations; we will not repeat it here.

3.3. Resolved observations

When the solar image is resolved many more degrees can be detected making the data analysis somewhat more complicated. In order to extract a single l, m mode from resolved observations, one has to apply a specific spatial filter or weight to the velocity or intensity images. Most often these weights are such that imperfect isolation of the l, m mode is achieved; especially because the most commonly used filters (spherical harmonics) are *not* orthogonal over half a sphere. This leads to the existence of other modes in the Fourier spectrum generated for a given l, m filter. Therefore, the observed Fourier spectrum is a linear combination of the modes to be detected. This linear combination of the modes can be understood as modes leaking into each other spectrum: this is represented by the so-called *leakage* matrix. These leakages will produce correlations between the different Fourier spectra. These correlations will modify the statistics of the Fourier spectra, such that their power spectra cannot be described as a χ^2 with 2 degrees of freedom. Therefore the statistics of the $2l+1$ power spectra of a given l cannot be derived from the product of $2l+1$ χ^2 with 2 degrees of freedom as in Appourchaux et al. (1995). Nevertheless, the real and imaginary parts of the Fourier spectra will still be normally distributed; in other words, the Fourier spectra have a *multi-normal distribution* defined by a covariance matrix. This fact will be used to derive the statistics of the observation. The covariance matrix is the sum of the noise and mode covariance matrices, which are not necessarily the same. Last but not least, the theoretical probability distribution has to be generated using the previous covariance matrix.

In summary, to understand the statistics of resolved observation, one has to follow four steps:

- Compute leakage matrices,
- Compute mode covariance matrices (related to the leakage),
- Compute noise covariance matrices,
- Generate the likelihood from the theoretical probability distribution.

Each step is described in detail hereafter.

3.3.1. Leakage matrices

Due to the spherical symmetry of the Sun, the most likely weights to be used to isolate the modes are the spherical harmonics $Y_{l,m}$. Here we generalize the approach to any weight $W_{l,m}$. The result is the observation of Fourier spectra $y_m^l(\nu)$ that are related to what we want to detect, i.e. the Fourier spectra of the individual Fourier spectrum $x_{m'}^{l'}(\nu)$, by the so-called leakage matrix (Schou 1992; Schou & Brown 1994). The following expression can be derived for as many different degrees as needed; for simplicity we wrote it for 2 different degrees l, l' as:

$$\boldsymbol{y} = \mathcal{C}^{(l,l')}\boldsymbol{x} \tag{12}$$

where $\boldsymbol{x}(\nu)$ and $\boldsymbol{y}(\nu)$ are 2 complex vectors made each of $2l+2l'+2$ component: $2l+1$ components for l, $2l'+1$ components for l' and $\mathcal{C}^{(l,l')}$ is the leakage matrix of both l and l'. The dimension of $\mathcal{C}^{(l,l')}$ is $(2l+2l'+2)\times(2l+2l'+2)$. The coefficient of the leakage matrix can be computed as:

$$\mathcal{C}^{(l,l')}_{m,m'} = \frac{b^{(l,l')}_{m,m'}}{b^{(l',l')}_{m',m'}} \tag{13}$$

with:

$$b^{(l,l')}_{m,m'} = \int_{\mathcal{D}} \frac{W^*_{l,m}(\theta,\phi)}{n_{l,m}} \tilde{Y}_{l',m'}(\theta,\phi) A(\theta,\phi) \sin\theta \mathrm{d}\theta\mathrm{d}\phi \tag{14}$$

where $m=-l,\ldots,l$, $m'=-l',\ldots,l'$, $*$ denotes the complex conjugate, θ,ϕ are the angles in a spherical coordinate system, $\mathcal{D}$ is the integration domain, $\tilde{Y}_{l',m'}$ is the generalized velocity or intensity perturbation of the mode (l',m'). The $\tilde{Y}_{l',m'}$ are not necessarily the usual spherical harmonics $Y_{l',m'}$. For instance, the horizontal component of the velocity perturbation, and the intensity perturbation due the distortion of the the surface by the modes are both expressed as derivative of spherical harmonics. $A(\theta,\phi)$ is an apodization function, $n_{l,m}$ is a sensitivity correction factor associated with $W_{l,m}$. The ratio ensures that $\mathcal{C}^{(l,l)}_{m,m}=1$. The apodization function A is the product of 3 different function as:

$$A(\theta,\phi) = A_{\mathrm{n}}(\theta,\phi) A_{\mathrm{d}}(\theta,\phi) A_{\mathrm{a}}(\theta,\phi) \tag{15}$$

A_{n} is the natural apodization function due to the way the images are obtained: for intensity this is the limb darkening ($I(\mu)$), and for velocity the projection factor ($\mu=\sin\theta\cos\phi$). A_{d} is the data analysis apodization: for data re-mapped on the Sun's surface it is unity; for no re-mapping, it is the projection factor ($\mu=\sin\theta\cos\phi$). A_{a} is the artificial apodization that can take into account the non-linear velocity (or intensity) response of the instrument over the solar disk, or can help to reduce limb effects. Here we must point out that the leakage matrix has a useful property such as:

$$\mathcal{C}^{(l,l')}_{m,m'} = \mathcal{C}^{(l',l)*}_{m',m} \frac{b^{(l,l)*}_{m,m}}{b^{(l',l')}_{m',m'}} \frac{b^{(l,l')}_{m,m'}}{b^{(l',l)*}_{m',m}}. \tag{16}$$

It shows that $\mathcal{C}^{(l,l')}$ is in general *not* hermitian nor symmetrical. Nevertheless, when $W_{l,m}=\tilde{Y}_{l,m}$, it is possible with a proper sensitivity factor correction of $W_{l,m}$ to have such a property. In this case the sensitivity correction is given by:

$$n_{l,m} = \sqrt{\int_{\mathcal{D}} \tilde{Y}^*_{l,m}(\theta,\phi)\tilde{Y}_{l,m}(\theta,\phi) A(\theta,\phi)\sin\theta\mathrm{d}\theta\mathrm{d}\phi} \tag{17}$$

which is the "natural" normalization factor of the perturbation $\tilde{Y}_{l,m}$. Of course in this latter case, we have:

$$\mathcal{C}^{(l,l')}_{m,m'} = \mathcal{C}^{(l',l)*}_{m',m}. \tag{18}$$

Unfortunately, the leakage matrix does not always have such a nice property, especially because $W_{l,m}\neq\tilde{Y}_{l,m}$. This was the case for the ground-based Luminosity Oscillations Imager (LOI) (Appourchaux et al. 1994) and for the GONG instrument (Hill 1997, private communication). In both cases, this is *not* produced by the observation techniques but by the data analysis techniques.

If the weight functions $W_{l,m}$ and the observed perturbations $\tilde{Y}_{l,m}$ have the same symmetry properties as the spherical harmonics $Y_{l,m}$ (or if $W_{l,m}=\tilde{Y}_{l,m}=Y_{l,m}$), the leakage matrix is real as shown by Schou (1992). In addition the leakage elements of $\mathcal{C}^{(l,l')}_{m,m'}$ are zero if $l+m+l'+m'$ is odd; this is the case when the Sun is *not* tilted with respect to the observer's axis of reference ($P=0$, $B=0$). If the axes of reference of $W_{l,m}$ differ from that of the $Y_{l,m}$ these 2 properties can be lost. For instance, an incorrect orientation of the Sun axis with respect to the detector axis could lead to a complex leakage matrix; or a Sun seen at an angle $B\neq 0$ give a real leakage matrix with non-zero elements with $l+m+l'+m'$ odd. This latter property has been used by Gizon et al. (1997) to infer the inclination of the Sun's core.

Equation (13) is valid when the size of the pixel is small compared with the spatial scale of the degree. When the pixels are larger, one should write the following:

$$\mathcal{C}^{(l,l')}_{m,m'} = \frac{n_{l',m'}}{n_{l,m}} \frac{\sum_i w_i^{(l,m)*}\tilde{y}_i^{(l',m')}}{\sum_i w_i^{(l',m')*}\tilde{y}_i^{(l',m')}} \tag{19}$$

where the $\tilde{y}_i$ are given by:

$$\tilde{y}_i^{(l',m')} = \int_{\mathcal{D}_i} \tilde{Y}^{m'}_{l'}(\theta,\phi) A(\theta,\phi)\sin\theta\mathrm{d}\theta\mathrm{d}\phi \tag{20}$$

where $\mathcal{D}_i$ is the area defined by the i-th pixel and $w_i^{(l,m)}$ is the weight applied to the i-th pixel to extract the l,m mode. Equation (19) is the more general form used for the LOI (Appourchaux & Andersen 1990). As a starting point, the $w_i^{(l,m)}$ can also be taken as the $\tilde{y}_i^{(l,m)}$.

3.3.2. p-mode covariance matrix

To compute the covariance of the complex vector $\boldsymbol{y}(\nu)$ as a real number we form the vector $\boldsymbol{z}_{\boldsymbol{y}}(\nu)$ defined as:

$\boldsymbol{z}^{\mathrm{T}}_{\boldsymbol{y}}(\nu) = (\mathrm{Re}(\boldsymbol{y}^{\mathrm{T}}), \mathrm{Im}(\boldsymbol{y}^{\mathrm{T}}))$.

In absence of noise, the covariance matrix $\mathsf{M}(\nu)$ of the vector $\boldsymbol{z}_{\boldsymbol{y}}(\nu)$ can be generated using a complex notation:

$$\mathsf{M}^{(l,l')}(\nu) = \begin{pmatrix} \mathcal{M}_r(\nu) & \mathcal{M}_i(\nu) \\ -\mathcal{M}_i(\nu) & \mathcal{M}_r(\nu) \end{pmatrix}. \tag{21}$$

$\mathsf{M}^{(l,l')}$ is a super matrix where $\mathcal{M}_r(\nu)$ and $\mathcal{M}_i(\nu)$ are the real and imaginary parts of a complex matrix $\mathcal{M}^{(l,l')}$ which elements are given by:

$$\mathcal{M}^{(l,l')}_{m,m'}(\nu) = \sum_{l''=l,l'} \sum_{m''=-l''}^{l''} \mathcal{C}^{(l'',l')}_{m'',m'} \mathcal{C}^{(l'',l)*}_{m'',m} f^{l''}_{m''}(\nu) \tag{22}$$

where $f^{l''}_{m''}(\nu)$ is the variance of the l'',m'' mode which profile is given by Eq. (11), in which ν_0 is a function of m.

The real and imaginary parts of Eq. (22) will give respectively the covariance of the real (or imaginary) part of $\boldsymbol{y}$, and the covariance between the real and imaginary part of $\boldsymbol{y}$. It is obvious from Eq. (22) that $\mathcal{M}^{(l,l')}$ is hermitian.

Schou (1992) gave an equation similar to Eq. (22) for a real leakage matrix and for a single degree. Here we add a subtlety to the formulation of Schou (1992), the matrix $\mathsf{M}^{(l,l')}(\nu)$ can be decomposed as follows:

$$\mathsf{M}^{(l,l')}(\nu) = \begin{pmatrix} \mathsf{v}(\nu) & \mathsf{w}(\nu) \\ -\mathsf{w}(\nu) & \mathsf{v}(\nu) \end{pmatrix} \begin{pmatrix} \mathsf{v}^{\mathrm{T}}(\nu) & -\mathsf{w}^{\mathrm{T}}(\nu) \\ \mathsf{w}^{\mathrm{T}}(\nu) & \mathsf{v}^{\mathrm{T}}(\nu) \end{pmatrix} \tag{23}$$

where T is the transpose of a matrix. The elements of v and w are given by:

$$\mathsf{v}^{(l,l')}_{m,m'}(\nu) = \sqrt{f^l_m(\nu)}\mathrm{Re}(\mathcal{C}^{(l,l')}_{m,m'}) \tag{24}$$

$$\mathsf{w}^{(l,l')}_{m,m'}(\nu) = \sqrt{f^l_m(\nu)}\mathrm{Im}(\mathcal{C}^{(l,l')}_{m,m'}). \tag{25}$$

We will see later on that this decomposition is of prime importance for understanding the statistics of the observation.

3.3.3. Noise covariance matrix

Unfortunately, the observed vector $\boldsymbol{y}(\nu)$ include a noise contribution. Due to the way the data are combined, the noises between the different $2l+2l'+2$ components of this vector are also correlated. Schou (1992) gave the correlation matrix when the filter used are spherical harmonics $Y_{l,m}$. A more general formulation can be written as:

$$\mathsf{B}^{(l,l')}(\nu) = \begin{pmatrix} \mathcal{B}_r(\nu) & \mathcal{B}_i(\nu) \\ -\mathcal{B}_i(\nu) & \mathcal{B}_r(\nu) \end{pmatrix} \tag{26}$$

$\mathsf{B}^{(l,l')}$ is a super matrix where $\mathcal{B}_r(\nu)$ and $\mathcal{B}_i(\nu)$ are the real and imaginary parts of the complex matrix $\mathcal{B}^{(l,l')}$. The dimension of $\mathcal{B}^{(l,l')}$ is $(2l+2l'+2)\times(2l+2l'+2)$. Its elements are given by:

$$\mathcal{B}^{(l,l')}_{m,m'} = \int_{\mathcal{D}} \frac{W^*_{l,m}(\theta,\phi)}{n_{l,m}} \frac{W_{l',m'}(\theta,\phi)}{n_{l',m'}} a(\theta,\phi)\sin\theta \mathrm{d}\theta\mathrm{d}\phi \tag{27}$$

with

$$a(\theta,\phi,\nu) = A^2_{\mathrm{a}}(\theta,\phi)A^2_{\mathrm{d}}(\theta,\phi)\sigma^2_{\odot}(\theta,\phi,\nu) \tag{28}$$

where a is an apodization function which characterizes through $\sigma^2_{\odot}(\theta,\phi,\nu)$ how the noise varies over the solar image, assuming that the noise is uncorrelated between different points on the Sun; $A_{\mathrm{a}}, A_{\mathrm{d}}$ are defined in Eq. (15). When the instrumental noise is low, a is derived from the characteristics of the solar noise. The evaluation of $\mathcal{B}^{(l,l')}$ is less straightforward than that of $\mathcal{C}^{(l,l')}$ because we need to know a model of the solar noise. An easier way to understand the noise correlation is to built the ratio covariance matrix or "pseudo" noise leakage matrix $\mathcal{R}$ as:

$$\mathcal{R}^{(l,l')}_{m,m'} = \frac{\mathcal{B}^{(l,l')}_{m,m'}}{\mathcal{B}^{(l',l')}_{m',m'}}. \tag{29}$$

Here we can see the similarity between $\mathcal{R}$ and $\mathcal{C}$. In velocity, the granulation noise is rather low at the center of the disk and then increases towards the limb; the meso- and super-granulation exhibits somewhat different or complementary center-to-limb variations. In intensity, the granulation noise is a function of the number of granules; the noise is larger at the center of the disk and decreases slowly towards the limb. In addition the solar noise in intensity has no contribution from mesogranulation (Fröhlich et al. 1997), making the spatial dependence of the noise almost independent of frequency across the p-mode range. This is not the case in velocity where mesogranulation still contributes to the noise in the p-mode range. Therefore in intensity the apodization a is closer to A than in velocity, making the ratio covariance matrix $\mathcal{R}^{(l,l')}$ very close to the leakage matrix $\mathcal{C}^{(l,l')}$. Although $\mathcal{R}^{(l,l')}$ is not mathematically useful, it is a matrix easy to visualize and understand (See Part II). The ratio matrix has some properties of the leakage matrix like being not necessarily hermitian. This is not the case of $\mathcal{B}^{(l,l')}$ which is hermitian by definition.

Again, when the size of the pixel is large compared with the spatial scale of the degree, Eq. (27) is rewritten as follows:

$$\mathcal{B}^{(l,l')}_{m,m'}(\nu) = \sum_i w_i^{*(l,m)} w_i^{(l',m')} b_i(\nu) \tag{30}$$

where b_i is the variance of the noise of pixel i. Equation (30) is the more general form used for the LOI.

3.3.4. Probability density of the observation and likelihood

The statistical distribution of the Fourier spectra or of the vector $\boldsymbol{z_y}$ is a multi-normal distribution. The probability density is given by:

$$p_{\boldsymbol{y}}(\nu) = \frac{\mathrm{e}^{-\frac{1}{2}\boldsymbol{z}^{\mathrm{T}}_{\boldsymbol{y}}(\nu)\mathsf{V}^{-1}(\nu)\boldsymbol{z_y}(\nu)}}{(2\pi)^{d/2}\sqrt{|\mathsf{V}(\nu)|}} \tag{31}$$

where d is the number of elements of $\boldsymbol{z_y}$, V is a short notation for the following matrix: $\mathsf{V}^{(l,l')}(\nu) = \mathsf{M}^{(l,l')}(\nu) + \mathsf{B}^{(l,l')}(\nu)$; this is the matrix given by the sum of the p-mode and noise covariance matrix; the p modes and the noises are assumed to be independent of each other. The matrix $\mathsf{V}^{(l,l')}(\nu)$ can also be built from sub-matrices as: $\mathcal{V}^{(l,l')} = \mathcal{M}^{(l,l')} + \mathcal{B}^{(l,l')}$; as a result $\mathcal{V}^{(l,l')}$ is also hermitian. Equation (31) is the most general formulation for any multi-normal distribution with a given covariance matrix V (Kendall & Stuart 1967).

Using Eq. (31), we can write the likelihood L of an observation of $\boldsymbol{z_y}(\nu_i)$ at N different frequencies ν_i as given by:

$$L^{(l,l')}_{\boldsymbol{y}} = \prod_{i=1}^{N} \frac{\mathrm{e}^{-\frac{1}{2}\boldsymbol{z}^{\mathrm{T}}_{\boldsymbol{y}}(\nu_i)\mathsf{V}^{-1}(\nu_i)\boldsymbol{z_y}(\nu_i)}}{(2\pi)^{d/2}\sqrt{|\mathsf{V}(\nu_i)|}}. \tag{32}$$

We assumed that the frequency bins are independent of each other. This is the case when the data have no gaps. For unresolved observation having gap, the expression of

the likelihood becomes extremely complicated as shown by Gabriel (1994). For resolved observation having gaps, as for the LOWL data of Tomczyk et al. (1995), it is impracticable to use the full formulation of the likelihood: Tomczyk et al. (1995) used Eq. (32) as an approximation for fitting the LOWL data.

In principle, given the observed vector $\boldsymbol{y}$, it is always possible in the absence of noise to recover the vector $\boldsymbol{x}$. Due to the presence of noise only a solution close to the ideal one can be found that will minimize the correlation between the components. Provided that the leakage matrix can be inverted, we have by analogy to Eq. (12):

$$\tilde{\boldsymbol{x}} = \mathcal{C}^{-1}\boldsymbol{y} \tag{33}$$

where $\mathcal{C} = \mathcal{C}^{(l,l')}$. Then we can write a similar equation for $\boldsymbol{z_y}$ and $\boldsymbol{z_{\tilde{x}}}$ as:

$$\boldsymbol{z_{\tilde{x}}} = \mathsf{C}^{-1}\boldsymbol{z_y} \tag{34}$$

where C is defined as:

$$\mathsf{C}^{(l,l')}(\nu) = \begin{pmatrix} \mathcal{C}_r(\nu) & \mathcal{C}_i(\nu) \\ -\mathcal{C}_i(\nu) & \mathcal{C}_r(\nu) \end{pmatrix} \tag{35}$$

$\mathsf{C}^{(l,l')}$ is a super matrix where $\mathcal{C}_r$ and $\mathcal{C}_i$ are the real and imaginary parts of the complex matrix $\mathcal{C}^{(l,l')}$. Using Eq. (34) to replace $\boldsymbol{z_y}$ by $\boldsymbol{z_{\tilde{x}}}$ in Eq. (32) we can rewrite this latter as:

$$L_{\boldsymbol{y}}^{(l,l')} = \prod_{i=1}^{N} \frac{\mathrm{e}^{-\frac{1}{2}\boldsymbol{z}_{\tilde{\boldsymbol{x}}}^{\mathrm{T}}(\nu_i)\mathsf{V}'^{-1}(\nu_i)\boldsymbol{z}_{\tilde{\boldsymbol{x}}}(\nu_i)}}{(2\pi)^{d/2}\sqrt{|\mathsf{V}'(\nu_i)|}} \frac{1}{|\mathsf{C}|} = \frac{1}{|\mathsf{C}|^N} L_{\tilde{\boldsymbol{x}}}^{(l,l')} \tag{36}$$

with V' given by:

$$\mathsf{V}' = \mathsf{C}^{-1}\mathsf{V}\mathsf{C}^{\mathrm{T}^{-1}} = \mathsf{C}^{-1}\mathsf{M}^{(l,l')}\mathsf{C}^{\mathrm{T}^{-1}} + \mathsf{C}^{-1}\mathsf{B}^{(l,l')}\mathsf{C}^{\mathrm{T}^{-1}}. \tag{37}$$

We recognize in Eq. (36) the probability density of the vector $\boldsymbol{z_{\tilde{x}}}(\nu)$ to a constant (i.e. $|\mathsf{C}|^{-N}$). As a matter of fact, it is well known that using a linear transformation similar to that of Eq. (34) will produce the new covariance matrix V' of $\boldsymbol{z_{\tilde{x}}}$ as written in Eq. (37) (Davenport & Root 1958). It can be easily shown using Eqs. (23) and (37) that the matrix $\mathsf{D}(\nu) = \mathsf{C}^{-1}\mathsf{M}^{(l,l')}\mathsf{C}^{\mathrm{T}^{-1}}$ is diagonal and its element are given by:

$$\mathsf{D}_{m'',m''}(\nu) = f_{m''}^{l''}(\nu) \tag{38}$$

where $l'' = l$ or l' and $m'' = -l'', \ldots, l''$. Therefore Eq. (37) is the sum of a diagonal matrix representing the correlation between the p modes; and of a new noise covariance matrix representing the correlation of the components of the vector $\tilde{\boldsymbol{x}}$ after the transformation of Eq. (33). It means that $\tilde{\boldsymbol{x}}$ has no correlation due to the p modes as we could expect from Eq. (33): the leakage matrix of $\tilde{\boldsymbol{x}}$ is the identity matrix. In summary, *there is no gain in fitting data for which the leakage matrix is the identity matrix: the 2 approaches are identical.* The main problem is really to know the leakage matrices, not only theoretically but also experimentally: this is the subject of the Part II.

It can be derived from Eq. (37) that it is also possible to remove correlation due to the noise by replacing C by a proper matrix associated with $\mathsf{B}^{(l,l')}$. The derivation of this matrix is given in Appendix A.

3.3.5. The use of the likelihood in practice

When a single degree is observed, it is quite simple to maximize the likelihood of Eq. (32) using $\boldsymbol{y}$, or using $\tilde{\boldsymbol{x}}$ as in Eq. (36). For low degree and low frequency modes, this is possible for $l = 0, 2, 3$. As soon as the mode linewidth increases, at high frequencies, the assumption of a single degree is not valid anymore. For example, $l = 0$ and $l = 1$ overlap with $l = 2$ and $l = 3$, respectively. At high frequencies, the effect of the aliasing degree should be taken into account.

For the other low degree modes, the likelihood becomes somewhat more complicated. It is well known, that in the (m, ν) diagramme of $l = 1$, there are leaks coming from other degrees. The $l = 6$ and $l = 9$ modes overlap with the $l = 1$, while the $l = 3$ modes overlap only at higher frequencies when the linewidth is larger than about 5 μHz. In the (m, ν) diagramme of $l = 4$, there are leaks of $l = 7$ and vice versa (Appourchaux et al. 1997). The leaks have severe effects on determination of the p-mode parameters of the $l = 1$. When many degrees are overlapping, one should use Eq. (32) using the covariance matrix for l and l'. Nevertheless, we do not advice to do so for fitting the p modes; it has some severe computer speed penalty. Instead we advice to clean the data by inverting the full leakage matrix taking into account the effects of the various degrees on each other, in a similar way to Eq. (33). For example for $l = 1$, one should compute the leakage matrix on a sub-space of degrees namely for $l = 1$, 6 and 9. These 3 degrees interact strongly in the Fourier spectra. For $l = 4$ and $l = 5$ one should compute the leakage matrix on sub-spaces for $l = 4$ and 7, and for $l = 5$ and 8. The advantage of this direct cleaning is to replace the original aliasing degrees by new aliasing degrees which are further away, in frequency, from the modes to be fitted. This technique has been applied to the LOI and GONG data, and is developed in Part II.

Last but not least, when the signal-to-noise ratio is high (i.e. we neglect $\mathsf{B}^{(l,l')}$ in Eq. (37)), the elements of the vector $\boldsymbol{z_{\tilde{x}}}(\nu)$ are all independent of each other, leading to a statistical distribution which is a product of χ^2 with 2 degree of freedom. This is an approximation which is useful and less incorrect that using this statistics for the GONG data for the vector $\boldsymbol{z_y}(\nu)$ as in Hill et al. (1996).

4. Monte-Carlo simulations

4.1. Why are they needed?

Before applying Eq. (32) to real data, it is always advisable to test the power of MLE on synthetic data, i.e. performing Monte-Carlo simulations. They are not merely for playing games; these simulations are real tools for understanding what we fit and how we fit it. Assuming that the statistics of the real solar spectra is known, performing Monte-Carlo is useful for the following reasons:

– Assessing the model of the mode and noise covariance
– Assessing the statistical distribution of the parameters
– Assessing the precision of parameters.

First, the model of the covariances can be imperfect. The effect of an imperfect knowledge of the covariance can help us understand how these will influence the determination of the parameters, i.e. deriving the sensitivity of the systematic errors to this imperfect knowledge. Second, the parameters derived by the MLE should have the desirable properties of having a normal distribution; if not we advise to apply a change of fitted parameters. For example, as we will see later on, we do not fit the linewidth itself but the log of the linewidth. A normal distribution is necessary to derive meaningful error bars, this is the assumption behind Eq. (5). Third, in order to be able to derive a good estimate of the error bars using one realization, the standard deviation of a large sample of fitted parameters should be equal to the mean of formal errors return by the fit (See Eq. (4)).

4.2. Generation of synthetic data for the LOI

The performance of this instrument has been described in Appourchaux et al. (1997). Briefly, it is a small instrument made of 12 pixels for detecting solar intensity fluctuations. The p-mode signals were generated in the Fourier spectra by using the following:

$$\boldsymbol{y}(\nu) = \mathcal{C}^{(l,l)}\boldsymbol{x}(\nu) + \sum_{i=1}^{N_{\rm pix}} \tilde{\boldsymbol{y}}_i^l p_i \tag{39}$$

where $\boldsymbol{y}$ is the observed vector of $2l+1$ Fourier spectra, $\mathcal{C}^{(l,l)}$ is the leakage matrix given by Eq. (19), $\boldsymbol{x}$ is a complex random vector with $2l+1$ components (each component represents the signal of an l, m mode, with uncorrelated real and imaginary part), $\tilde{\boldsymbol{y}}_i^l$ are computed as in Eq. (20) using spherical harmonics, and p_i is the noise for a given pixel i. The variance of the real or imaginary part of the m-th component of $\boldsymbol{x}$ is given by $f_m^l(\nu)$; the mean of $\boldsymbol{x}$ is 0. The function $f_m^l(\nu)$ describes the profile of each m which is displaced from m by an amount which is given by:

$$\nu_m = \nu_0 + l\sum_{i=1}^{5} a_i \mathcal{P}_i^{(l)}(m/l) \tag{40}$$

where the $\mathcal{P}_i^{(l)}$ are derived from the Clebsch-Gordan coefficients, the expression of which can be found in Ritzwoller & Lavelly (1991); they are normalized such that $\mathcal{P}_i^{(l)}(1) = 1$. Here we assumed a common linewidth for the l, n mode, and different amplitudes for the $2l+1$ components. The profile are symmetrical in the shape of a lorentzian.

The variance of the pixel noise is assumed to be the same for the pixels with the same shape. The mean of the pixel noise is 0. For the LOI with its 12 pixels, there are 3 different shapes giving 3 independent noises.

After generating the synthetic signals according to Eq. (39), the data are fitted by minimizing the likelihood of Eq. (32). Figure 1 shows an example of Fourier spectra generated synthetically. The typical signal-to-noise ratio in the power spectra is about 20-30. The frequency resolution is equivalent to 4 months of data. We performed 1000 simulations of the spectra.

4.3. Results

4.3.1. For the nominal leakage matrix

The data are fitted assuming a perfect knowledge of the leakage and noise covariance matrices, i.e. we know what we fit. Figure 2 shows the distribution of the fitted parameters: the central frequency, splitting, log(linewidth), 3× log(amplitude), 3× log(pixel noise). For the last 7 parameters, we fit the log of the parameter because this transformation give a statistical distribution closer to a normal distribution (or log-normal distribution). It can be observed that the parameters derived are in most cases unbiased. Figure 3 shows the distribution of the error bars returned by the fit. In most case the mean of the error bars (returned by the fit) is not very different from the 1-σ deviation of the parameter distribution. Similar simulations have been performed for various degree (up $l = 3$). They show the same typical results as for Figs. 2 and 3, i.e. the fitted parameters are not, or weakly, biased, and the error bars returned by the fit give a good estimate of the real error bars.

4.3.2. Influence of a wrong leakage matrix

As was shown by Eq. (36), fitting p-mode spectra for which the leakage matrix is explicitly diagonal is equivalent to fitting p-mode spectra for which the matrix is *not* diagonal. Of course, it is always possible to construct data with a purely diagonal leakage matrix using Eq. (33), but we do so assuming that we know the leakage matrix $\mathcal{C}$. As a matter of fact, what matters is not to have the identity matrix as leakage matrix, but more the knowledge of the latter.

Hereafter, we have investigated the influence of a wrongly assumed leakage matrix on the fitted parameters of $l = 1$. We made 100 realizations and change the leakage parameter between $m = -1$ and $m = +1$ by ±50% from a nominal value for the LOI of 0.45. Figure 4 shows the influence of varying the assumed leakage element on the fitted parameters. It is quite interesting to note that the inferred central frequency is insensitive to mistakes in the leakage matrix. The linewidth becomes underestimated when the error is larger than 20%, while the amplitudes become overestimated. The most important result is the fact that the systematic error made on the splitting is not linear but quadratic. This systematic error can become as large

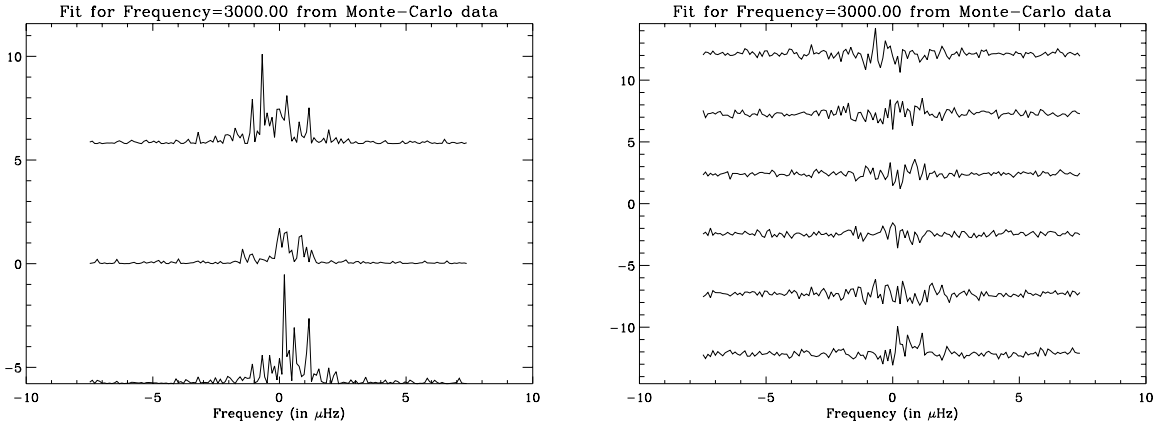

Fig. 1. (Left) Power spectra of a synthetic $l = 1$ as it would be observed by the LOI. The frequency resolution corresponds to 4 months of data. The signal-to-noise ratio is about 20-30. The traces from bottom to top corresponds to $m = -1$, 0, +1. (Right) Fourier spectra for $l = 1$ (same data). The first, third and fifth traces from the bottom represents the real part of the spectrum of $m = -1, 0$ and 1, respectively; the other traces are the imaginary parts. The leakage between $m = -1$ and $m = +1$ is 0.45 in the Fourier spectra

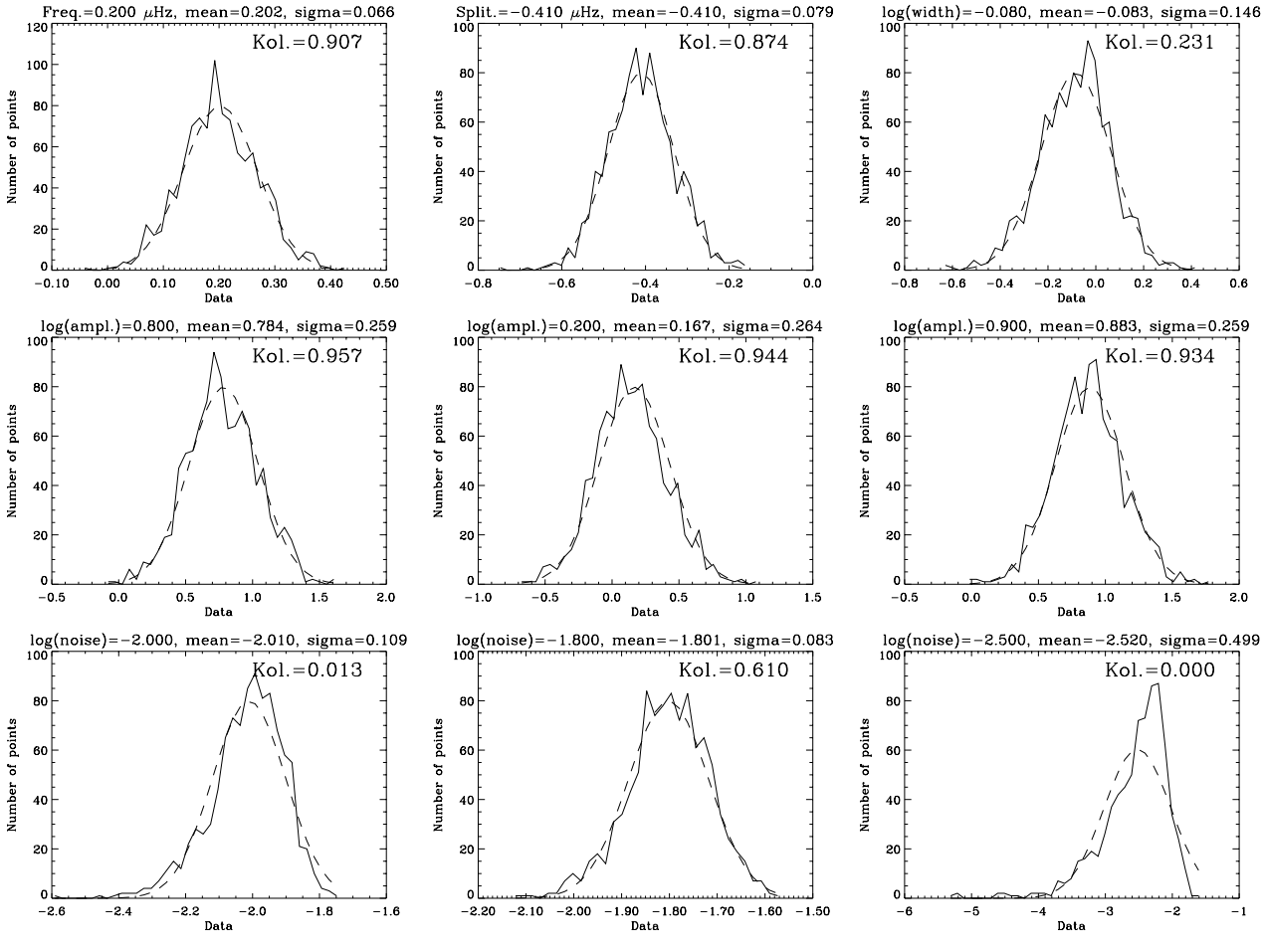

Fig. 2. Histograms for the fitted parameters: (Plain line) Data, (Dashed line) Normal distribution with the same mean and σ as the fitted parameters. (Top) Frequency (in μHz), splitting a_1 (in μHz), log(γ) (γ in μHz); (Middle) log(Amplitude) for $m = -1$, 0, 1; (Bottom) log(pixel noise). For each histogram, the target value, the mean fitted value and the 1-σ fitted valued are displayed. The Kolmogorov-Smirnov test (Kol.) is displayed for each histogram; a number close to 0 show that the distribution is not normal

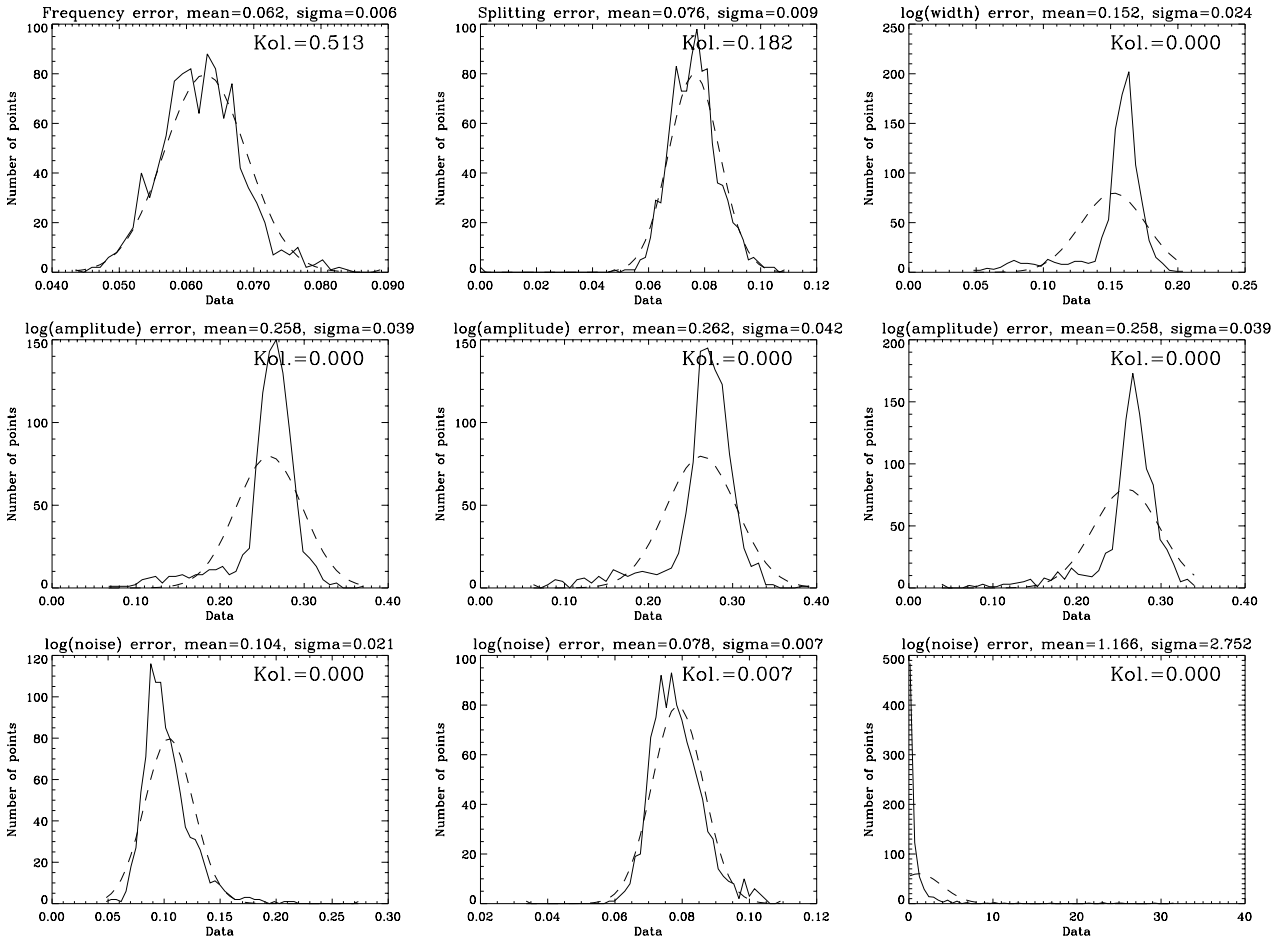

Fig. 3. Histograms for the error bars: (Plain line) Data, (Dashed line) Normal distribution with the same mean and σ. (Top) Frequency error (in μHz), splitting a_1 error (in μHz), log(γ) error (γ in μHz); (Middle) log(Amplitude) error for $m = -1$, 0, 1; (Bottom) log(pixel noise) error. For each histogram, the target value, the mean fitted value and the 1-σ fitted valued are displayed. The Kolmogorov-Smirnov test is displayed for each histogram; a number close to 0 show that the distribution is not normal

as the error bars. For example, with 1 year of LOI data and averaging over 10 modes, the error bars on the mean splitting is about 15 nHz; this should be compared to a systematic error of 10 nHz for an error of 10% of the $l = 1$ leakage elements.

Another test similar to that of the $l = 1$ was performed with the $l = 2$ mode. We have assumed that all the off-diagonal elements of the leakage matrix were wrong by the same fixed amount. Figure 5 shows the results only for the splitting coefficients (from a_1 to a_4). The other parameters linewidth, amplitudes and noises behave in the same manner as for $l = 1$. The systematic error on the splitting has also the same quadratic dependence as for $l = 1$. For $l = 2$ the splitting error bars are typically $\sqrt{5}$ smaller than for $l = 1$. In this case the systematic errors become larger than the error bars, and therefore start to influence the inverted solar rotation.

It means that it is quite easy to underestimate the splitting whenever we under- or overestimate the leakage element. As a matter of fact, this behaviour was also found in the GONG data for $l = 1$ and 2 (Rabello-Soares & Appourchaux 1998, in preparation). On the other hand, errors in the leakage matrix will not result in overestimating the splitting. If the splitting is overestimated, the most likely source should be the presence of other degrees not taken into account in the analysis.

We also checked the correlation of the splitting coefficients derived for $l = 2$. Figures 6 and 7 show respectively the variance and the covariance of the splitting coefficients as a function of the leakage elements error. It can be concluded that the splitting coefficients become correlated only when a large overestimation of about 50% is made for the off-diagonal leakage elements. This result is only valid when fitting Fourier spectra. For other methods, such as fitting power spectra, possible correlation amongst the splitting coefficients could have drastic consequences for the inverted solar rotation profiles.

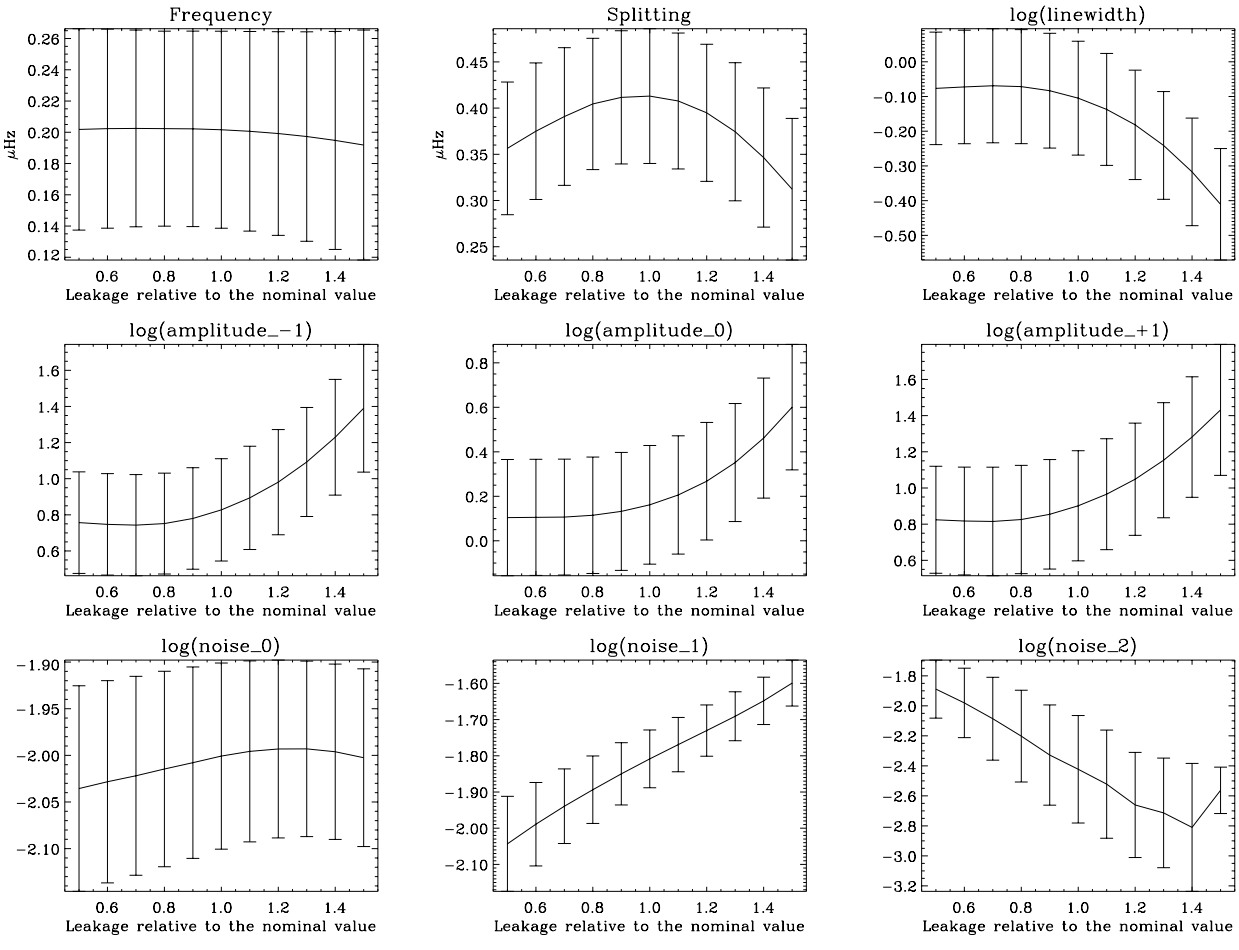

Fig. 4. Influence of the fitted parameters to relative changes of the assumed leakage element between $m = -1$ and $m = +1$ for $l = 1$. (Top) Frequency, splitting a_1, log(γ); (Middle) log(Amplitude) for $m = -1$, 0, 1; (Bottom) log(pixel noise). The target parameters are the same as for Fig. 2. Please note the parabolic shape for the splitting

4.3.3. Comparison with other methods

We have also performed Monte-Carlo simulations to compare the different fitting techniques commonly used. For each simulation of a mode, the data were fitted in 3 different ways:

- Assuming that the $2l + 1$ power spectra are independent of each other and are not influenced by m leaks, i.e. a single mode is present for a given m. This is the way the GONG data are commonly fitted.
- Assuming that the $2l + 1$ power spectra are independent of each other but are influenced by m leaks, i.e. we use only the diagonal of the mode covariance matrix. This is the way the LOI data were fitted by Appourchaux et al. (1995).
- Assuming that the $2l + 1$ Fourier spectra are dependent of each other and are influenced by m leaks. This is the way described in this paper after the work of Schou (1992).

Figure 8 shows the results of this comparison only for the splitting which is the parameter the most sensitive to the fitting way. The splittings derived by the GONG fitting way are obviously underestimated. This underestimation will eventually disappear with the degree but for $l = 1$ the bias is unacceptable. The splittings derived using the old LOI way are slightly overestimated with a bias of about 10 nHz for $l = 1$. Although this bias is not substantial for the LOI data, it can be of the same order of magnitude as the error bars for instrument with better signal-to-noise ratio than used in the simulations, such as GONG, and for observation time longer than these simulations. Last but not least, the Fourier spectra fitted according to the guidelines given in this paper provides a splitting without substantial bias and also with smaller error bars. This latter way of fitting will considerably improve the consistency of the splittings measured.

5. Conclusion

We have given a step by step recipe for fitting (m, ν) Fourier spectra. If one wants to implement similar fitting technique, one should compute, first the

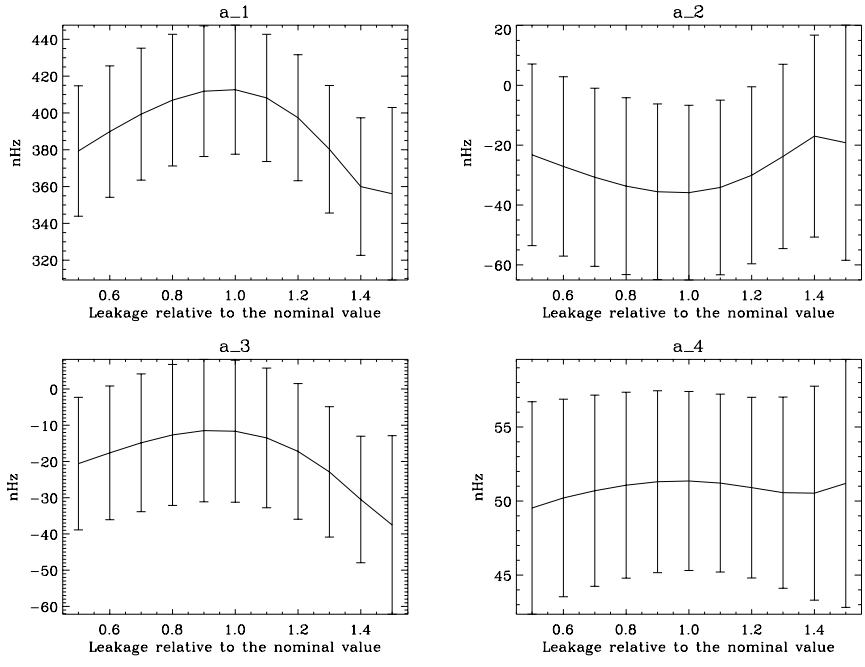

Fig. 5. Influence of the fitted splitting parameters to relative changes of the assumed of the assumed off-diagonal leakage element for $l = 2$. (Top, left) a_1, target value: 410 nHz; (Top, right) a_2, target value: -30 nHz; (Bottom, left) a_3, target value: -10 nHz; (Bottom, right) a_4, target value: $+50$ nHz

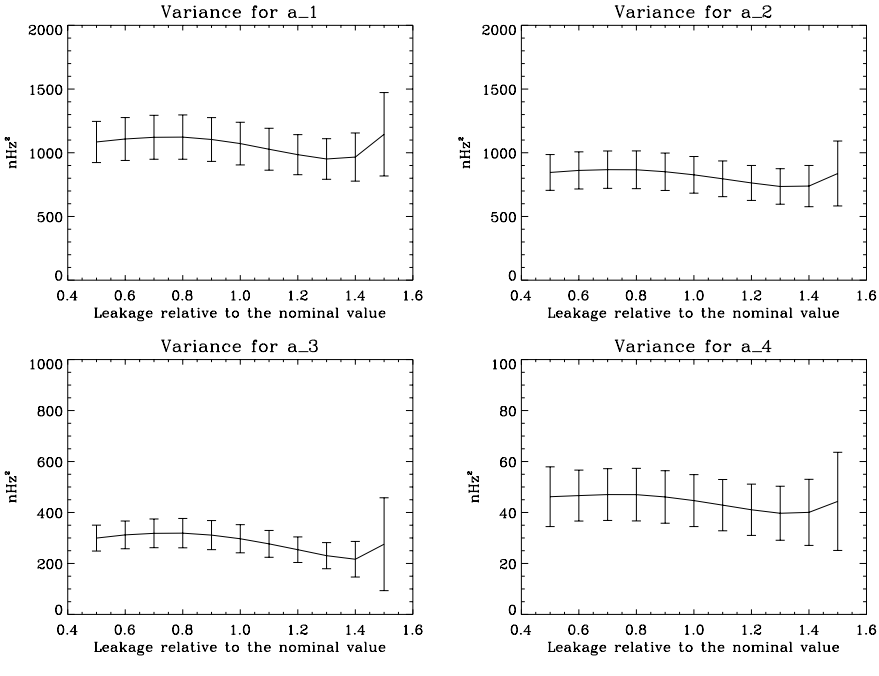

Fig. 6. Diagonal elements of the covariance matrix of the splitting coefficient, for $l = 2$. They are given as a function of the relative change of the assumed off-diagonal leakage element. (Top, left) For a_1; (Top, right) For a_2; (Bottom, left) For a_3; (Bottom, right) For a_4

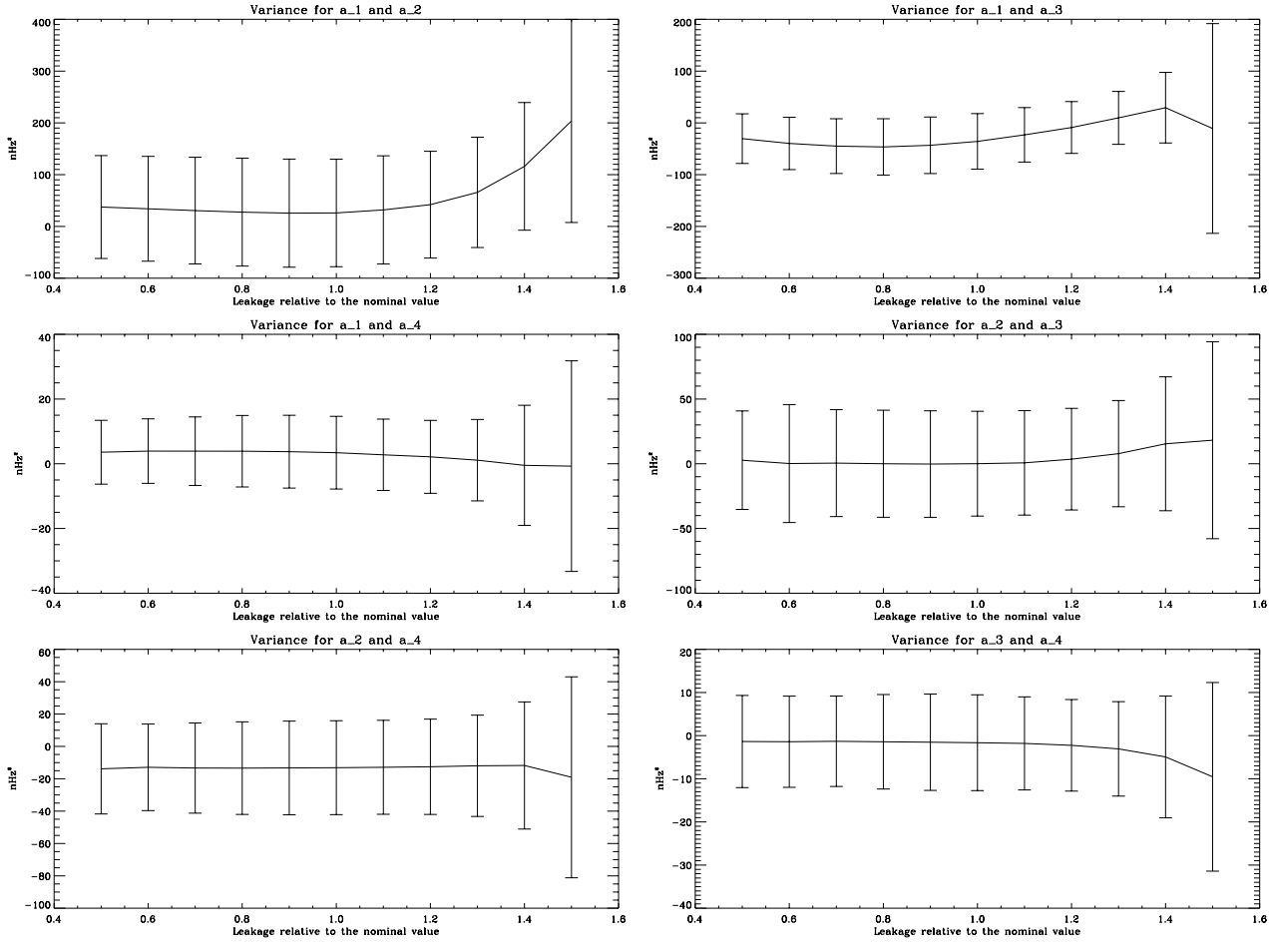

Fig. 7. Off-diagonal elements of the covariance matrix of the splitting coefficient, for $l = 2$. They are given as a function of the relative change of the assumed off-diagonal leakage element. (Top, left) For a_1 and a_2; (Top, right) For a_1 and a_3; (Middle, left) For a_1 and a_4; (Middle, right) For a_2 and a_3; (Bottom, left) For a_2 and a_4; (Bottom, right) For a_3 and a_4

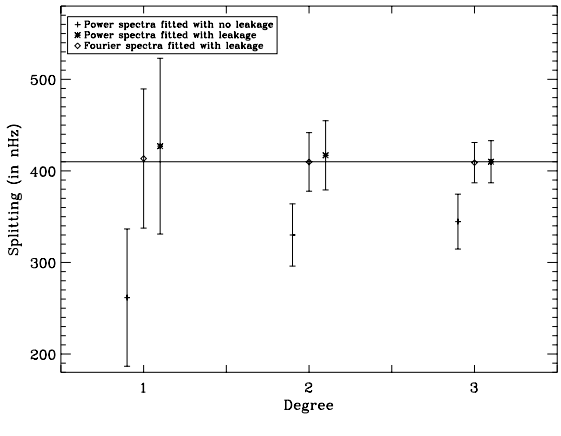

Fig. 8. Comparison of low-degree splittings measured using 1000 Monte-Carlo simulations by 3 different fitting techniques. The nominal splitting is 410 nHz. The + is the technique commonly used by GONG, the asterisk is the technique used by Appourchaux et al. (1995), the diamond is the technique described in this paper and also used for the SOI/MDI data. The error bars are the formal error bars for a single realization

leakage matrices according to Eqs. (13) and (14), second the mode covariance matrices with Eq. (22) (or using Eq. (23)), third the noise covariance matrices with Eq. (27) using a model of solar noise, fourth compute the likelihood function using Eq. (32). The use of Monte-Carlo simulations will ensure the success of the implementation. Routines for fitting p-mode Fourier spectra are available as freeware on the VIRGO home page: virgo.so.estec.esa.nl; they are written in the IDL macro language.

Last but not least, Eq. (36) showed us the equivalence between fitting data for which the leakage matrix is not the identity, and fitting data for which it explicitly is. This last statement is true provided that we know perfectly well the leakage matrix. In this case the p-mode parameters fitted using MLE are not, or very weakly, biased, and have minimum variance. For instance, we showed for the splitting that other commonly fitting methods result either in a bias and/or larger formal errors. We have also studied the effect of an imperfect knowledge of the leakage matrix on the fitted parameters, in order to derive the effect of systematic errors on the most interesting parameters:

the splitting and mode frequency. We found that the central frequency is insensitive to systematic errors in the leakage matrix, while the splitting coefficients (a_i) have a quadratic dependence upon those errors. These systematic errors will have influence on the inverted solar rotation profiles.

Finally, we would like to stress again that the correct statistical treatment of the p-mode data is of vital importance for deducing unbiased p-mode parameters.

Acknowledgements. Many thanks to Takashi Sekii for constructive comments on the manuscript, and for extensive cyberspace chatting :-). We are grateful to the referees for their constructive comments.

Appendix A:

The purpose of this appendix is to show that using a proper matrix $\mathsf{C_B}$, the noise covariance matrix of Eq. (37) given by:

$$\mathsf{B}'^{(l,l')} = \mathsf{C_B}^{-1}\mathsf{B}^{(l,l')}\mathsf{C_B}^{\mathrm{T}^{-1}} \tag{A1}$$

can have a diagonal form. The matrix $\mathsf{B}^{(l,l')}$ can be diagonalized and we can write.

$$\mathsf{B}^{(l,l')} = \mathsf{P}^{-1}\mathsf{b}^{(l,l')}\mathsf{P}^{\mathrm{T}^{-1}} \tag{A2}$$

where $\mathsf{b}^{(l,l')}$ is diagonal and P is an orthogonal matrix ($\mathsf{P}^{-1} = \mathsf{P}^{\mathrm{T}}$). Replacing Eq. (A2) into Eq. (A1), we have:

$$\mathsf{B}'^{(l,l')} = \mathsf{C_B}^{-1}\mathsf{P}^{-1}\mathsf{b}^{(l,l')}\mathsf{P}^{\mathrm{T}^{-1}}\mathsf{C_B}^{\mathrm{T}^{-1}}. \tag{A3}$$

Since $\mathsf{B}^{(l,l')}$ is positive definite all its eigenvalues are positive, therefore the square root of $\mathsf{b}^{(l,l')}$ is defined. Therefore if we apply the following transformation to the data:

$$\mathsf{C_B} = \mathsf{P}^{-1}\sqrt{\mathsf{b}^{(l,l')}} \tag{A4}$$

we can rewrite Eq. (A3) as:

$$\mathsf{B}'^{(l,l')} = \mathsf{I} \tag{A5}$$

where I is the identity matrix. So replacing C in Eq. (33) by $\mathsf{C_B}$ will have the effect of removing the artificial correlation due to the noise, and also of performing a normalization. We should point out that the transformation matrix $\mathsf{C_B}$ that can achieve this is not unique, and any multiplication by an orthogonal matrix will achieve this. Nevertheless, we give a solution to the problem which can be solved as an eigenvalue and eigenvector problem. The transformation given above does not remove the artificial correlation due the p modes but more or less preserve it. This can have some useful application when one wants to produce spectra with uncorrelated noise but with correlated p-mode signals.

References

Anderson E.R., Duvall Jr. T.L., Jefferies S.M., 1990, ApJ 364, 699

Appourchaux T., Andersen B.N., 1990, Sol. Phys. 128, 91

Appourchaux T., Andersen B.N., Fröhlich, Jiménez A., Telljohann U., Wehrli C., 1997, Sol. Phys. 170, 27

Appourchaux T., Gough D.O., Sekii T., Toutain T., 1997, IAU 181, Nice, Provost J. and Schmider F.-X. (eds.)

Appourchaux T., Gizon, 1998 (in preparation)

Appourchaux T., Toutain T., Telljohan U., Jiménez A., Andersen B.N., 1995, A&A 294, L13

Appourchaux T., Rabello-Soares M.C., Gizon L., 1998 (submitted to A&A)

Brownlee K.A., 1965, Statistical Theory and Methodology in Science and Engineering, 2nd edition. John Wiley and Sons, New York

Chang, 1996, PhD Thesis. University of Cambridge

Christensen-Dalsgaard J., Gough D.O., 1982, MNRAS 198, 141

Davenport W.B. Jr., Root W.L., 1958, An Introduction to the Theory of Random Signals and Noise. McGraw-Hill Eds., New York

Duvall T.L. Jr., Harvey J.W., 1986, Seismology of the Sun and the Distant Stars. Dordrecht, D. Reidel, p. 105

Frieden B.R., 1983, Probability, Statistical Optics, and Data Testing: A Problem Solving Approach. Springer-Verlag, Berlin

Fröhlich C., Andersen B.N., Appourchaux T., et al., 1997, Sol. Phys. 170, 1

Gabriel M., 1994, A&A 287, 685

Gizon L., Appourchaux T., Gough D.O., 1997, Proceedings of the Kyoto General Assembly

Hill F., Stark R.T., Stebbins R.T., et al., 1996, Sci 272, 1292

Kendall M.G., Stuart A., 1967, The advanced theory of Astrophysics: Inference and relationship, Vol. II, 2nd edition. Butler and Tanner Ltd. Eds., London

Kumar P., Franklin J., Goldreich P., 1988, ApJ 328, 879

Quenouille M.H., 1956, Biometrika 43, 353

Rabello-Soares M.C., Appourchaux T., 1998 (in preparation)

Rabello-Soares M.C., Roca Cortés T., Jiménez A., Appourchaux T., Eff-Darwich A., 1997, ApJ 480, 840

Ritzwoller M.H., Lavely E.M., 1991, ApJ 369, 557

Schou J., 1992, PhD thesis, On the analysis of helioseismic data, Aarhus University, Aarhus

Schou J., Brown T.M., 1994, A&AS 107, 541

Tomczyk S., Schou J., Thompson M.J., 1995, ApJ 488, L57

Toutain T., Appourchaux T., 1994, A&A 289, 649

Toutain T., Gouttebroze P., 1994, A&A 268, 309

Wilks S.S, 1938, Ann. Math. Stat. 9, 60

Woodard M., 1984, PhD Thesis, University of California, San Diego